Path sampling calculation of methane diffusivity in natural gas hydrates from a water-vacancy assisted mechanism

Baron Peters[1,3,*], Nils E.R. Zimmermann[1,4], Gregg T. Beckham[2,5], Jefferson W. Tester[2], Bernhardt L. Trout[2,*]

[1]*Centre Européen de Calcul Atomique et Moléculaire (CECAM), Ecole Normale Supérieure, 46 Allée d'Italie, 69364 Lyon, France*

[2]*Department of Chemical Engineering, Massachusetts Institute of Technology, Cambridge, MA 02139*

current addresses:

[3]*Chemical Engineering, University of California, Santa Barbara, CA 93106-5080*

[4]*Hamburg University of Technology (TUHH), Chemical Reaction Engineering, Eißendorfer Str. 38, D-21073 Hamburg, Germany*

[5]*National Bioenergy Center, National Renewable Energy Laboratory, Golden, CO 80401*

**Corresponding author email: trout@mit.edu, baronp@engineering.ucsb.edu*

RECEIVED DATE

Path sampling study of methane diffusion in hydrate

ABSTRACT

Increased interest in natural gas hydrate formation and decomposition, coupled with experimental difficulties in diffusion measurements, makes estimating transport properties in hydrates an important technological challenge. This research uses an equilibrium path sampling method for free energy calculations [R. Radhakrishnan and T. Schlick, *J. Chem. Phys.* **121** 2436 (2004)] with reactive flux and kinetic Monte Carlo simulations to estimate the methane diffusivity within a structure I gas hydrate crystal. The calculations support a water-vacancy assisted diffusion mechanism where methane hops from an occupied "donor" cage to an adjacent "acceptor" cage. For pathways between cages that are separated by five-membered water rings, the free energy landscape has a high barrier with a shallow well at the top. For pathways between cages that are separated by six-membered water rings, the free energy calculations show a lower barrier with no stable intermediate. Reactive flux simulations confirm that many reactive trajectories become trapped in the shallow intermediate at the top of the barrier leading to a small transmission coefficient for these paths. Stable intermediate configurations are identified as doubly occupied off-pathway cages and methane occupying the position of a water vacancy. Rate constants are computed and used to simulate self-diffusion with a kinetic Monte Carlo algorithm. Self-diffusion rates were much slower than the Einstein estimate because of lattice connectivity and methane's preference for large cages over small cages. Specifically, the fastest pathways for methane hopping are arranged in parallel (non-intersecting) channels, so methane must hop via a slow pathway to escape the channel. From a computational perspective, this paper demonstrates that equilibrium path sampling can compute free energies for a

broader class of coordinates than umbrella sampling with molecular dynamics. From a technological perspective, this paper provides one estimate for an important transport property that has been difficult to measure. In a hydrate I crystal at 250K with nearly all cages occupied by methane, we estimate $D \approx 7 \cdot 10^{-15}$ X m^2/s where X is the fraction of unoccupied cages.

Keywords: path sampling, diffusion, methane, hydrate, transmission coefficient, kinetic Monte Carlo, free energy calculation, Bolas, carbon sequestration

INTRODUCTION

Natural gas hydrates are crystalline inclusion compounds with an H_2O lattice that forms a periodic array of cages with each cage large enough to contain a single methane molecule.[1-3] Structure I methane hydrates are found in marine sediments below the sea floor and under the permafrost in quantities that make hydrates a potential energy source and hydrocarbon feedstock.[1,4] Furthermore, hydrates have safety and economic advantages over transporting stranded natural gas.[5] Interesting strategies for using hydrates have been proposed.[1] For example, methane might be producible in usable quantities from natural gas hydrates in located in the arctic and marine sediments, and deep ocean hydrates near warm places could conceivably be harvested and used for refrigeration, gas, and water.[6] In addition, some speculate that CO_2 can be sequestered within natural gas hydrates.[7] One strategy to sequester CO_2 is to inject high pressure CO_2 into natural gas hydrate deposits and recover the displaced CH_4 as fuel, as both experiments[7] and simulations[8] demonstrate that CO_2 displaces CH_4 from the hydrate

structure. For, methane production, hydrate mining, and CO_2 sequestration applications, the timescale for methane diffusion is an important variable.

Experiments on hydrates are difficult for several reasons.[1,9-12] The foremost difficulty in measuring diffusion rates *within* a hydrate crystal is that large single crystals of methane hydrate are difficult to grow and handle in the laboratory, and that grain size distributions in polycrystalline hydrates are generally sensitive to conditions of growth.[13,14] Indirect estimates of methane diffusion rates have been made by fitting models of hydrate growth.[9-11] However, apparent mass transfer rates in polycrystalline materials are sensitive to factors like sample grinding and grain morphology.[15] Grinding could affect both grain sizes and the nature of grain boundaries, so it is difficult to separate contributions to the apparent rate of mass transfer through polycrystalline hydrates. The apparent rate of mass transfer into a polycrystalline sample could be limited by diffusion along grain boundaries, by diffusion into the hydrate lattice, or in exchange processes, by crystal growth kinetics in a mechanism where the CH_4 hydrate decomposes and a CO_2 hydrate is reconstructed.[15]

Understanding the mass transfer and exchange mechanisms would resolve critical questions that surround potential carbon sequestration and methane recovery strategies. For example, Ripmeester and coworkers observe that CH_4 remains in the hydrate even as CH_4 becomes infinitely dilute in the atmosphere.[15] Thermodynamics predicts an ever-increasing chemical potential driving force ($\Delta\mu_{CH4,hydrate} = \Delta\mu^0_{CH4,hydrate} + RTlnP_{CH4}$) that pushes CH_4 out of the hydrate as the surrounding atmosphere becomes CH_4 depleted. Thus, mass transfer limitations may be important in hydrates.

This paper investigates one of the possible diffusion mechanisms that might explain observations like that of Ripmeester and coworkers.[15] We use an equilibrium path sampling method based on Bolas,[16] reactive flux simulations,[17] and kinetic Monte Carlo[18] to obtain the self diffusion constant of methane molecule in a natural gas hydrate. Our hypothesized mechanism for diffusion is thermally activated hopping from an occupied cage to an adjacent vacant cage. As proposed previously for the CO_2 diffusion mechanism in hydrates,[19] we hypothesize that a water vacancy between the donor and acceptor cages facilitates methane hopping. Our hypothesis implies a diffusion rate that depends on temperature and methane vacancy concentration. One consequence of concentration dependent diffusivity is the possibility of singular diffusion where wetting-front behavior could arrest the mass transfer process in a non-equilibrium state.[20] We emphasize that further simulations and experiments are also needed to investigate alternative diffusion mechanisms like Bjerrum defect assisted diffusion,[21,22] and crystal decomposition-reconstruction mechanisms like those involved in hydrate formation from ice.[9-11]

METHODOLOGY

Force field parameters and simulation details: Previous simulations have used *ab initio* calculations[23-26] and empirical force fields[8,19,27-35] to model hydrates. TIP4P water[36] describes the known phases of ice,[37,38] and recent studies show that it accurately describes the host lattice of the hydrate.[8,28,36] The TIP4P potential was used for the internal degrees of freedom of water and for water-water interactions. Long range electrostatics were treated using particle mesh Ewald summation with 32 k-points.[39] Internal degrees of freedom in CH_4 and CH_4-CH_4 interactions were modeled using the

OPLS[40] potential. The CH_4 and H_2O interactions were specially developed for methane hydrates by Anderson et al.[24,28] All simulations were performed in CHARMM on a cubic system of 8 unit cells (2x2x2) of structure I methane hydrate. Water orientations were selected with the algorithm of Buch et al.[41] Simulations were performed at two temperatures, 225 K and 250 K, using the Nose-Hoover thermostat.[42]

To approximate a constant pressure of 40 atm, the average box length for a fully occupied structure I methane hydrate ($CH_4 \cdot 6H_2O$) was computed for a 1 ns trajectory with an extended Lagrangian barostat.[43] We performed simulations to calibrate the size of a cubic box as a function of temperature. The hydrate remains stable for a nanosecond at temperatures as high as 325 K at 40 atm, but these high temperature structures are probably metastable. We chose the temperatures 225 K and 250 K which are slightly below the melting temperature of TIP4P water based on the work of Vega et al.[38] At P=40 atm the box size is 23.33±0.05 Å at T=225 K, and 23.39±0.05 Å at T=250 K, in reasonable agreement with the experimental lattice constants.[1]

Subsequent calculations to compute rate constants were performed with NVT simulations using a cubic simulation box at the mean length from the NPT simulations at the corresponding temperature. Thermal expansion was incorporated in the simulation box size, ensemble effects generally diminish with system size,[44] and solids have small compressibility, so the free energy barriers computed within the NVT ensemble were interpreted as approximate[44] Gibbs free energies.

Finally, we note that lattice distortions associated with the transition state along a hopping pathway could be affected by their own periodic images. Larger scale

simulations, e.g. a 27 unit cell simulation (3x3x3), would be needed to determine whether finite size effects are important.

Spherical bipolars for reaction coordinates and for detecting water vacancies: If methane diffuses by hopping between adjacent cages of the hydrate lattice, then there are three pathways to consider between adjacent cages in structure I.[1] These are:

"L6L" from large donor cage to a large acceptor cage through a water vacancy in a six-membered water ring

"S5L" from small donor cage to large acceptor cage through a water vacancy in a five-membered water ring

"L5L" from large donor cage to large acceptor cage through a water vacancy in a five-membered water ring

Figure 1 shows configurations along the S5L pathway with the methane in the donor (small) cage, between the donor and acceptor cages, and in the acceptor (large) cage.

<< Figure 1 >>

Bipolar coordinates (q , θ) as shown in Figure 2 were used to describe the position of the methane molecule relative to the centers of the donor and acceptor cages. The reaction coordinate is q and θ is a measure of deviation from the straight line path between the initial and final cage centers. These coordinates are convenient because they describe all three pathways (S5L, L5L, and L6L) between cages in the structure I hydrate lattice.

<< Figure 2 >>

For each configuration sampled, the donor and acceptor cage centers are needed to compute q and θ. The cage centers were found using ghost atoms that avoid all atoms *except for the five atoms of the hopping, or "tagged", methane molecule*. The ghost potential $v(r)$, defined in Figure 3, is truncated at the minimum to leave a repulsive $1/r^2$ core that avoids any atom within 5Å (except for the tagged methane). Because the cages are 3-4Å in radius, the surrounding water molecules "push" the ghost atoms to the center of the acceptor and donor cages. The ghost particles do not alter the dynamics or energetics of the actual methane hydrate system. They are a fictitious device for obtaining the acceptor and donor cage centers as foci for the bipolar coordinates. For each configuration sampled, the positions $\mathbf{r}_{g1}$ and $\mathbf{r}_{g2}$ of two ghost atoms were optimized using the potential in equation 1.

$$\begin{aligned} V(\mathbf{r}_{g1}, \mathbf{r}_{g2} \mid \mathbf{r}^N) = & \sum_{\text{untagged k}} v(|\mathbf{r}_k - \mathbf{r}_{g1}|) \\ & + \sum_{\text{untagged k}} v(|\mathbf{r}_k - \mathbf{r}_{g2}|) + \frac{1}{2}(|\mathbf{r}_{g1} - \mathbf{r}_{g2}| - r_{EQ})^2 \end{aligned} \tag{1a}$$

and

$$v(r) = \begin{cases} 5/r^2 - 2/r + 1/5 & r < 5 \\ 0 & r \geq 5 \end{cases} \tag{1b}$$

<< Figure 3 >>

The last term in the ghost potential restrains the distance between the acceptor and donor cage centers near their equilibrium distances. The restraint helps prevent one ghost atom from hopping into a neighboring cage during the simulations. The equilibrium distances r_{EQ} in the restraints were the average distances from an unbiased simulation between two unrestrained ghost atoms in adjacent acceptor-donor cages with a water

vacancy between the cages. The equilibrium distances for the L6L, L5L, and S5L cages are shown in Table 1.

<< Table 1 >>

Table 1 also includes two values of q ($q_{\min}$ and $q_{\max}$) and one value of θ ($\theta_{\min}$) for each hopping pathway. These values specify a region between donor and acceptor cages as shown in Figure 4. Our hypothesis requires a water vacancy between the donor and acceptor cages, so one water molecule must be missing from the region of Figure 4. Note that the region is actually a volume of rotation about the donor-acceptor axis. For the L6L hop, the region should contain 6-1 = 5 water molecules, and for L5L or S5L hops the region should contain 5-1 = 4 water molecules.

<< Figure 4 >>

Testing the water vacancy hypothesis requires a sampling method that can include a constraint on the number of water molecules in the water vacancy region. Furthermore, q and θ are iteratively defined variables that are obtained through a numerical optimization of ghost atom positions. Importance sampling by simple molecular dynamics would be convenient, but forces corresponding to the constraints and the q and θ variables are not easily computed. To circumvent this problem we introduce a version of the Bolas[16] algorithm with Aimless Shooting[45,46] moves to improve sampling efficiency.

Equilibrium path sampling: Path sampling originated in the study of rare events, so path sampling might be viewed as synonymous with Transition Path Sampling (TPS).[47] However, Radhakrishnan and Schlick[16] showed that path sampling can also harvest an equilibrium ensemble for free energy calculations. Surprisingly few

investigators[16,46,48,49] have used the versatile and powerful Bolas algorithm for free energy calculations. This may be due to a historical identification of path sampling with TPS.[47] In the present paper we use a modified version of Bolas,[16] which might be called modified Bolas if desired, but we will call it Equilibrium Path Sampling (EPS) to emphasize the difference from TPS. The EPS algorithm described in this paper is operationally different from the original Bolas algorithm, but it still employs the fundamental idea of Bolas.[16] *We stress that unless EPS is being explicitly compared to the original[16] Bolas algorithm, all statements about EPS in this paper apply equally to the original Bolas method.*

Path sampling methods generate an ensemble of paths by repeatedly generating a path from the previous path and then accepting the path according to a Metropolis rule for the path weight in the desired ensemble.[47] TPS generates the ensemble of transition paths for a reaction by requiring paths to begin in the reactant state and end in the product state.[47] By instead requiring trajectories to visit a region R, EPS generates the ensemble of paths that visit R at equilibrium. Within the region R, configurations along these paths are therefore distributed according to the equilibrium distribution. Thus EPS can be used for free energy calculations.[16]

An advantage of EPS over Monte Carlo importance sampling[44] is that Newton's equations of motion naturally include the collective motions of a real system while Monte Carlo might require a sophisticated library of moves. When compared to molecular dynamics based umbrella sampling,[50] EPS replaces the need for an easily differentiable umbrella potential with a simple path acceptance criteria. Because EPS eliminates the need for a bias potential, molecular dynamics based importance sampling is no longer

restricted to easily differentiable coordinates like bond distances, angles, and dihedrals. Thus, EPS can extend the utility of molecular dynamics packages like AMBER,[51] CHARMM,[52] GROMACS,[53] and NAMD.[54]

Our version of EPS uses Aimless Shooting[45,46] instead of Shooting and Shifting[47] as used in the original Bolas algorithm.[16] Aimless Shooting trajectories diverge from one another quickly because the momenta are drawn fresh from the Boltzmann distribution whereas the original Shooting algorithm "aims" each new trajectory along the previous trajectory. Configuration sampling efficiency depends on both trajectory acceptance and the similarity of successive trajectories. Bolas trajectories can be extremely short (100fs in our study), so independent shooting momenta[45] may enhance configuration sampling. The EPS algorithm below samples the equilibrium distribution of configurations **x** within a region R.

1) select one of $(k+1)$-timeslices on the previous trajectory:

   $\mathbf{x}^{(o)}(0\Delta t)$, $\mathbf{x}^{(o)}(1\Delta t)$, …, or $\mathbf{x}^{(o)}(k\Delta t)$

2) select a random integer j between 0 and k. let the point selected in step (1) be timeslice $j\Delta t$ on a new trajectory: $\mathbf{x}^{(n)}(j\Delta t)$

3) select momenta **p** from the Boltzmann distribution and propagate the dynamical equations forward in time from $\mathbf{x}^{(n)}(j\Delta t)$ to $\mathbf{x}^{(n)}(k\Delta t)$. Also reverse the initial momenta **p** and propagate the equations of motion back to $\mathbf{x}^{(n)}(0\Delta t)$.

4) accept the new trajectory $\mathbf{x}^{(n)}(0\Delta t)$, $\mathbf{x}^{(n)}(1\Delta t)$, …, or $\mathbf{x}^{(n)}(k\Delta t)$ if any timeslice is in R.

Many accepted trajectories will extend beyond the window R, but these points are not distributed according to the equilibrium distribution. Therefore the windows should overlap so that the free energies from one window to another can be linked with a weighted histogram analysis.[55] An optimum trajectory length kΔt results from the cost of initiating molecular dynamics trajectories too frequently for short trajectories and at the other extreme from wasted molecular dynamics timesteps that extend beyond the region R. Also note that on steep portions of the free energy surface, it can be useful to reduce the number of timeslices per trajectory. This increases the trajectory acceptance rate by reducing the "wasted" fraction of the trajectories that extend beyond R. Our trajectories were all 100 fs long, with Δt=10 fs, and k=10. (Δt is the data collection interval, not the timestep). For each window, 20,000 accepted trajectories were collected, giving 220,000 configurations. However, not all of the 220,000 configurations are within R and the shooting points are redundant configurations. As in Monte Carlo sampling,[44] the most recent accepted trajectory should be recounted each time a trajectory is rejected.

RESULTS AND DISCUSSION

Free energy barrier for the "L6L" hop with no water vacancy: EPS was used to compute the free energy landscape in the (q, θ) coordinates for L6L hopping. For this calculation, *the full water lattice was included.* The free energy was sampled by dividing the space around the donor and acceptor cage centers into windows according to values of q. Figure 5 shows the free energy in two-dimensional Cartesian coordinates with lines of constant q and θ for reference. The free energy was computed only for positive q because the barrier should be approximately symmetric about q=0. The Jacobian factor was included in mapping the free energy from (q, θ) to (x, y) coordinates:

$$F(x,y)/kT=F(q,\theta)/kT+\ln|\partial(q,\theta)/\partial(x,y)| \quad (2)$$

where x and y are defined by $x = \sinh(q)/(\cosh(q)-\cos(\theta))$ and $y = \sin(\theta)/(\cosh(q)-\cos(\theta))$.

Because of its size, methane does not fit through the six-membered ring without distortion, so one hydrogen bond in the water ring breaks at the transition state and the methane takes a path that curves away from the straight line between the acceptor and donor cage toward the broken bond. This is reflected in the free energy landscape by a saddle (at q=0) that is offset from the donor acceptor axis at $\theta \approx 30°$. In Figure 6, the free energy is projected onto the single coordinate q revealing an activation energy of approximately $30kT$ at 250 K. The free energy reaches a minimum and then rises again at large values of q because of the diminishing volume between q and q+dq at large values of $|q|$. Note that Alavi and Ripmeester[26] found that H_2 easily passes through five and six membered water rings even when there is no water vacancy in the structure. A comparison of these results suggests that guest molecule size has a large effect on the diffusion mechanism and on the diffusion rate.

<< Figure 5 >>

<< Figure 6 >>

Concentration of water vacancies: Our hypothesis is that water vacancies facilitate diffusion. To test that hypothesis, we consider two pathways by which methane can hop from a donor cage to a vacant "acceptor" cage in the hydrate lattice:

(1) the methane plows through an intact clathrate cage. This mechanism corresponds to the free energy of Figures (5) and (6).

(2) the methane "waits" until a water vacancy appears between the donor and acceptor cages and then slips through the defect site with a reduced barrier.

For the second pathway, the rate of passage through a water vacancy defect must be multiplied by the fraction of time that the water vacancy is present in the donor-acceptor channel.

The free energy to form a water vacancy is related to the fraction of time that a water vacancy defect resides in the donor-acceptor channel. Thermodynamic integration,[44]

$$\Delta F = \int_0^1 d\lambda \left\langle \frac{\partial E}{\partial \lambda} \right\rangle_\lambda , \quad (3)$$

was used to compute the reversible work to create a water vacancy by scaling the partial charges and Lennard-Jones interaction parameters of one TIP4P water molecule by a factor λ. Demurov et al.[19] computed the concentration of water vacancies in a type-I hydrate using SPC/E water and by transferring the water molecule to an ideal gas phase. Our results are expected to differ from theirs because we have used TIP4P water and transferred the water to the stable phase of TIP4P water at the temperature and pressure of the simulation. The endstates of thermodynamic integration are depicted in Figure 7.

<< Figure 7 >>

From the work of Vega et al.[38] the melting point of TIP4P water at 40 atm can be estimated as 231 K±5 K. Thus, at 250 K the TIP4P water molecule was transferred from the hydrate phase to a TIP4P water bath at 250 K and 40 atm. At 225 K where TIP4P is stable as ice, the calculation is more complicated. The calculation *is not intended to compare the free energy to form a water vacancy in the hydrate with the free energy to fill a water vacancy in ice.* Therefore, the TIP4P water molecule was transferred from a hydrate at 225 K to a water bath at 232 K. The result was corrected by the free energy change to freeze (ΔG=zero) and cool the system with one additional water from 232 K to

225 K. ($S=S^o+C_p\ln[T/T^o]$ with $dG=-SdT$) For the correction, experimental values at 1 atm were used for the heat capacity and for S^o.[56] The difference between two Poynting corrections for pressurization and depressurization to and from 40 atm at 225 K and 232 K were ignored. The estimated free energy correction was nearly insignificant, 0.286 J/mol. Results are shown in Figure 8.

<< Figure 8 >>

At 250 K and 40 atm thermodynamic integration predicts that approximately 1 water molecule in the hydrate lattice per 74 is vacant. Further within the region of hydrate stability at 225 K and 40 atm, approximately 1 water in 211 is vacant. The 4.3*kT* and 5.3*kT* free energies required to create a vacancy in the hydrate at 250 K and 225 K must be included in comparing the barriers to methane diffusion via the water vacancy assisted and unassisted mechanisms.

Free energy barriers with a water vacancy: Figures 9(a), (b), and (c) show the free energy barriers for methane hopping with a water vacancy at 250 K in the regions listed in Table 1. The figures again include the Jacobian factor of equation (2) for transformation to Cartesian coordinates. The L6L pathway has a barrier of just 12.6*kT*, 17*kT* lower than the barrier for hopping with a water vacancy. With the 4.3*kT* units of free energy to create a water vacancy, the barrier for the hypothesized mechanism assisted by a water vacancy is still much lower than the barrier for the unassisted pathway.

The L5L and L6L barriers were computed by using symmetry across the q=0 isosurface. The S5L barrier is asymmetric, but it is similar to the L5L pathway because both have a broad, shallow intermediate at the top of the barrier. The intermediate

reflects configurations where the hopping methane molecule occupies the vacancy created by a missing water molecule or a neighboring cage to the side of donor-acceptor pathway. The intermediate configurations effectively create a doubly occupied cage[57] adjacent to both the donor and acceptor cages that is slightly stable. Figure 1 showed the configurations along the S5L pathway. Interestingly, the barriers are higher for the S5L and L5L pathways than for the L6L pathways.

<< Figure 9 >>

Transition state theory: The rate constants for individual hops can be obtained from the computed free energy barriers using transition state theory[58].

$$\mathrm{k_{TST}} = \frac{1}{2\mathrm{x_A}} \left\langle \delta[q - q^*] \right\rangle \left\langle \left| \dot{q} \right| \right\rangle_{q=q^*} \tag{4a}$$

where

$$\left\langle \left| \dot{q} \right| \right\rangle_{\mathrm{q=q^*}} = \frac{\left\langle \delta[q - q^*] \left| \dot{q} \right| \right\rangle}{\left\langle \delta[q - q^*] \right\rangle} \tag{4b}$$

and x_A is the equilibrium fraction of time the system spends on the reactant side of the barrier. $\left\langle \left| \dot{q} \right| \right\rangle_{q=q^*}$ can be estimated by averaging the Jacobian scalefactor[59] for the curvilinear spherical bipolar[60] reaction coordinate, $h_q=(r_{EQ}/2)/[cosh(q)\text{-}cos(\theta)]$:

$$\begin{aligned} \left\langle \left| \dot{q} \right| \right\rangle_{\mathrm{q=q^*}} &= \left\langle \left| \nabla_{\mathbf{xDA}} q(\mathbf{x},\mathbf{D},\mathbf{A}) \cdot \mathrm{d}(\mathbf{x},\mathbf{D},\mathbf{A}) / \mathrm{dt} \right| \right\rangle_{q=q^*} \\ &\approx \left\langle \left| \nabla_{\mathbf{x}} q \cdot \dot{\mathbf{x}} \right| \right\rangle_{q=q^*} = \sqrt{\frac{2kT}{\pi \mathrm{m}}} \left\langle \left\| \nabla_{\mathbf{x}} q \right\| \right\rangle_{q=q^*} \\ &= \sqrt{\frac{8kT}{\pi \mathrm{m}\, \mathrm{r_{EQ}}^2}} (\cosh(q^*) - \left\langle \cos(\theta) \right\rangle_{q=q^*}) \end{aligned} \tag{5}$$

Here **x, D**, and **A** are Cartesian vector positions of the methane molecule and the two ghost particles, respectively. The approximation assumes the ghost atoms, **D** and **A**, are

static and that flux across $q=q^*$ comes only from motion of the methane molecule itself, i.e. from d**x**/dt. r_{EQ} values are given in Table 1.

Numerical integration of $\cosh(q^*)-\cos(\theta)$ weighted by a histogram of θ-values on the surface $q=q^*$ gave approximately the value $\cosh(q^*)-\cos(\theta^*)$ where θ^* is the value of θ at the saddle point in the free energy landscape. Invoking this approximation and using units of time $\beta h = h/kT$, length $\lambda_T = h/(2\pi m kT)^{1/2}$, and mass m=16amu for methane as a united atom gives

$$\beta h \left\langle |\dot{q}| \right\rangle_{q=q^*} \approx 4(\cosh(q^*) - \cos(\theta^*))\lambda_T / r_{EQ}. \quad (6)$$

<< Table 2 >>

Table 2 summarizes the transition state theory parameters for equations 4 and 6. Rate constants are omitted from Table 2 because the relationship between equilibrium cage occupancy and hopping kinetics reveals a missing component of the rate constants.

The missing component is subtle, so we take some care to explain its origin. The probability to create a water vacancy depends mostly on the four strong hydrogen bonds that must be broken. However, the water molecule being removed also interacts with nearby methane molecules, four of them in a hydrate with full methane loading. In the situation relevant for hopping, one of the four methanes is missing, i.e. the vacant acceptor cage. Hopping via the water vacancy assisted mechanism can be envisioned to happen in three steps. For example, the S5L hop has the steps:

(1) Create a water vancancy defect between a small donor cage and a large acceptor cage.

(2) Hop between the donor and acceptor cages while the water vacancy defect persists. (this step corresponds to the free energy of Figure 9)

(3) Heal the water vacancy defect with the methane molecule in the large cage.

For the S5L hop, and for the L5S hop, the final and initial states are different, so the water vacancy formation and healing free energies do not cancel. However, the difference between water vacancy creation and healing free energies, combined with the free energy change in step (2), should be consistent with established relative occupation numbers.[1] To account for this we introduce the correction in equation 7 and Figure 10 shows its origin.

$$\eta = -\beta\Delta G^{H2O-vac}_{\text{"S" donor}} + \beta\Delta G^{H2O-vac}_{\text{"L" donor}} . \quad (7)$$

<< Figure 10 >>

The thermodynamic integration of Figure (8) provides the overall concentration of water vacancies, but η corrects for the difference between water vacancy concentrations around large and small cage methane vacancies. A simple model with small and large cages coupled to a constant chemical potential bath shows that a free energy for methane in the large cage that is $1.7kT$ lower than the free energy of methane in the small cage approximately reproduces empirical occupancy fits.[1]

The resulting correction η (η always smaller than $2kT$) can be subtracted from the forward S5L barrier, added to the backward (L5S) barrier, or partitioned with some portion of η subtracted from the forward S5L barrier and some portion added to the reverse barrier. The two extreme cases give a window of uncertainty in our predicted S5L and L5S barriers and also lead to the lower and upper estimates of the diffusivity in Figure 12. The correction η and the associated uncertainly for S5L and L5S hops is included in the rate constants of Table 4.

Transmission coefficients: The water molecules encountered between the donor and acceptor cages will disrupt the motion of the methane molecule as it travels along the reaction pathway. Furthermore, the S5L and L5L pathways each have a local free energy minimum at the top of their barriers. These intermediates can disrupt the barrier crossing dynamics and lower the rate constant relative to the transition state theory rate.[17,61-63] Reactive flux correlation functions[64] were computed to account for dynamical effects on the hopping rates. Initial configurations for trajectories were randomly selected from a pre-sampled set of 10,000 Boltzmann distributed transition states on $q(\mathbf{x})=q^*$ for each path using EPS. Figures 11(a), (b), and (c) show the reactive flux correlation functions, $\kappa(t)$, for the L6L, S5L, and L5L hops respectively. The separate contributions[64] to the reactive flux from trajectories that were initially crossing the transition state surface in the forward direction ($\kappa+$) and backward ($\kappa-$) directions are also shown. Figures 11(a), (b), and (c) also show swarms of trajectories initiated with Boltzmann distributed velocities from the transition state surfaces of the L6L, S5L, and L5L pathways.

<< Table 3 >>

The function $\langle H[q(t_{plateau})]\rangle_{q(0)=q^*}$ where $H[q]$ is the Heaviside function gives the fraction of trajectories from the initial swarm that commit to the product state. For the L6L hop, trajectories commit quickly and $\langle H[q(t_{plateau})]\rangle_{q(0)=q^*}$ is approximately 0.5. The short commitment time and ~50% split between donor and acceptor cages confirms the lack of a stable intermediate in the L6L free energy barrier. The L5L and S5L trajectories take longer to commit and $\langle H[q(t_{plateau})]\rangle_{q(0)=q^*}$ is significantly larger than 0.5. These "swarms" were started on the product-side rim of the intermediate basin. Half of these swarms initially commit to the product (acceptor) basin and the other halves enter

the stable intermediate state. The stable intermediate population then splits again leading to as much as 75% of the original swarm ultimately committing to the product basin. The features of the free energy surfaces in Figure 9 agree closely with the dynamical characteristics of the evolving swarm and the separate components of the reactive flux correlation function.

<< Figure 11 >>

Table 4 combines the transition state theory, reactive flux, thermodynamic integration results, and the empirical correction η into rate constants for each of the hopping pathways at 225 K and 250 K. For the dynamical factors at 225 K, the values of κ and $\beta h\langle|\dot{q}|\rangle_{q^*}$ were taken from the 250 K simulations but the value of $\beta h\langle|\dot{q}|\rangle_{q^*}$ was scaled by $(250/225)^{1/2}$ to account for the new temperature according to equation (5).

<< Table 4 >>

Kinetic Monte Carlo and methane self-diffusion: For any cage in the hydrate with no guest molecule, the guest molecules in adjacent (donor) cages can hop into the acceptor cage. The number of possible hopping events thus depends on the type of cage and the occupancy of neighboring cages. Small cages in the hydrate have 12 neighboring large cages all connected to the small cage via a five membered water ring. Large cages in the hydrate have 14 neighbor cages: six small cages and eight large cages.[1] Two of the eight neighboring large cages are connected via a six membered water ring, and the other six large cages are connected via a five-membered water ring.[1] The rate constant for hopping into a vacant cage depends on the donor and acceptor cages and the type of boundary that they share, i.e. S5L, L5S, L5L, or L6L. The rates computed above are used in a kinetic Monte Carlo (KMC) simulation of methane

diffusion. We assume the water vacancies diffuse much faster than the methane vacancies. This approximation is supported by the observation of spontaneous water vacancy migration in our simulations when we do not localize the water vacancy using the scheme depicted in Figure 4. Furthermore, Demurov et al.[19] showed that water vacancies diffuse rapidly in the hydrate lattice, and work by Davidson and Ripmeester[21] shows that water molecules are more mobile than guests.

The Gillespie algorithm[18] simulates diffusion by updating a list of possible hopping "reactions" after each hopping event. When a hop occurs, the list of vacant cages and their neighbor occupancies is updated to give a new list of possible reactions. The diffusion rate is then calculated from the Einstein diffusion relation: $\langle R^2 \rangle = 6Dt$. Simulations were conducted for 8x8x8 unit cells and 1,000,000 hopping events at various concentrations. Periodic boundary conditions were used, but net displacements were monitored without periodic boundary conditions to ensure that $\langle R^2 \rangle$ did not include finite size effects. Initial conditions were prepared with uniformly distributed vacancy patterns to ensure fast equilibration with no long lived gradients in the vacancy distribution. The systems were equilibrated for 1,000,000 hopping events before taking data. The results are shown in Figure 12. Diffusion rates are reported relative to the Einstein estimate:[19,44] $D = k_{L6L}^{250K} X(6A)^2$ where X is the fraction of methane vacancies and 6Å is the approximate distance for an L6L hop. The rates are nearly an order of magnitude slower than the Einstein estimate because of the hydrate lattice topology. The fastest L6L pathways are arranged in parallel (non-intersecting) lines in the hydrate. The diffusion along L6L pathways alone is therefore a one-dimensional diffusion process. To

change directions, a methane molecule must hop via one of the slower S5L or L5L pathways.

<< Figure 12 >>

At typical methane vacancy concentrations found in the hydrate our calculations predict a diffusion constant on the order of $10^{-15} m^2/s$, a few orders of magnitude faster than the (approximate) rate of methane diffusion in an ice-h crystal[10] and a few orders of magnitude slower than the rate of methane diffusion through polycrystalline ice[9,10] and hydrate layers.[11] This finding supports claims that the diffusion rates in polycrystalline ice and hydrates are dominated by diffusion along grain boundaries.[9-11] Interestingly, Klapp et al.[14] demonstrated a method to determine grain size distributions in natural gas hydrates. Comparison of methane diffusion rates through hydrate samples with different grain sizes may help determine the rate of diffusion in a pure crystal. Direct measurements of the methane diffusion rate may also be possible using new single crystal growth techniques.[65]

The self-diffusion constant is approximately proportional to the guest vacancy concentration over the range $0.02 < X < 0.1$, which corresponds to measured hydration numbers.[66-70] (The hydration number "n" in the expression $CH_4 \cdot nH_2O$ can be converted to a guest vacancy concentration X using the expression $n = 5.75/(1-X)$.) For small X, most of the vacant cages are small cages because of methane's affinity for large cages. For X near 0.25, methane vacancies will also become common in the large cages. This would facilitate diffusion by opening the L6L pathway, but hydrates with $X \geq 0.25$ are likely to be unstable. The relationship between the diffusion constant, lattice topology, and guest molecule affinity for large cages may have important implications for larger

molecules with a stronger preference for large cages. For example, CO_2 hydrates have mostly unoccupied small cages.[71] The ready availability of the S5L pathway may lead to a different relationship between diffusivity and guest occupancy in CO_2 hydrates. These effects have not been verified, but they are interesting questions for future work.

CONCLUSIONS

This paper uses an equilibrium path sampling approach[16] with reactive flux[64] and kinetic Monte Carlo[18] simulations to estimate the methane diffusion rate in structure I gas hydrates.[1] In a hydrate I crystal at 250K with nearly all cages occupied by methane, we estimate $D \approx 7 \cdot 10^{-15}$ X m^2/s where X is the fraction of unoccupied cages. At 225K we estimate $D \approx 1 \cdot 10^{-15}$ X m^2/s. The calculations support a diffusion mechanism where water vacancies in the hydrate lattice provide a geometric opening for methane to pass from an occupied "donor" cage to an adjacent "acceptor" cage.[19]

The free energy landscape reveals differences between the three pathways by which methane hops between different cages in the hydrate structure. The pathway between large cages that are separated by six-membered water rings ("L6L") has the smallest activation barrier and no stable intermediates along the pathway. Pathways between large cages separated by five-membered water rings ("L5L") have a large barrier with a shallow intermediate state at the top of the barrier. Reactive flux simulations[64] show that the intermediate leads to a low transmission coefficient. Structures associated with the intermediate state have methane occupying the position vacated by the water molecule, and methane creating a doubly occupied cage that is off-pathway from donor to acceptor. A similar high barrier with a shallow intermediate at the top of the barrier was found for the pathway between a large cage and a small cage in the hydrate.

Kinetic Monte Carlo simulations based on the computed rate constants showed that self-diffusion was nearly an order of magnitude slower than the Einstein estimate. The discrepancy was attributed to the connectivity of different pathways in the structure I hydrate lattice. Specifically, the fastest pathways for methane hopping are arranged in parallel (non-intersecting) lines in the hydrate. CH_4 must hop via one of the slower pathways to change directions. Because of the lattice connectivity and guest molecule preferences for large cages,[3] the diffusion rate is coupled nonlinearly to the concentration of guest molecule vacancies. The nonlinearity is small for methane which can fit in both small and large cages, but it may be pronounced for larger guest molecules with a stronger preference for large cages.

From a computational perspective, this paper demonstrates that EPS[16] can compute free energies for a broader class of coordinates than umbrella sampling with molecular dynamics.[50] Reactive flux correlation functions[17,64] provided dynamically correct rates and additional insight into the effects of a stable intermediate near the top of the activation barrier. Finally, kinetic Monte Carlo[18] simulations enabled an estimate of a technologically important diffusion constant that has been difficult to measure. We hope these calculations will stimulate efforts to measure diffusion rates within single hydrate crystals and further simulations to investigate other possible diffusion mechanisms.

ACKNOWLEDGEMENTS

BP and NZ are grateful to Berend Smit for mentorship, generous support, encouragement, and helpful suggestions. We also thank Brian Anderson for hydrate forcefield files. BP and NZ were supported at the CECAM by the EC through the Marie Curie EXT and EST Projects MEXTCT-2003-023311 and MEST-CT-2005-020491,

respectively. We thank Enitechnologie for support in addition to the Singapore-MIT Alliance for funding.

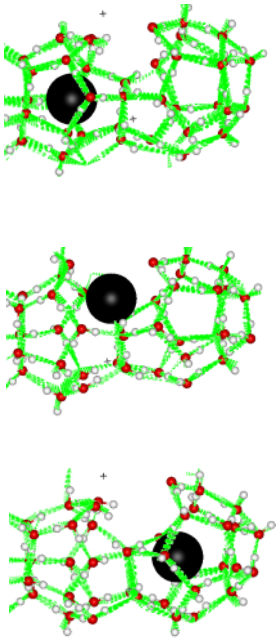

Figure 1: S5L hop showing the methane molecule (black) in the donor cage (S, top), between the cages (middle), and in the acceptor cage (L, bottom). Hydrogen atoms on the methane were omitted for clarity. Also note the missing water molecule between the two cages.

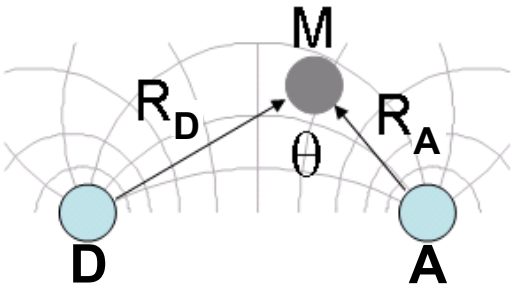

Figure 2: The coordinates $q = \ln[R_D/R_A]$ and θ = angle[DMA] describe the position of a methane molecule (M) with respect to ghost atoms A and D that occupy the initial (D) and final (A) cages. The plane between the two cages is the isosurface $q = 0$. Contours of θ are shown in 30° intervals and contours of q are shown in intervals of 1/2.

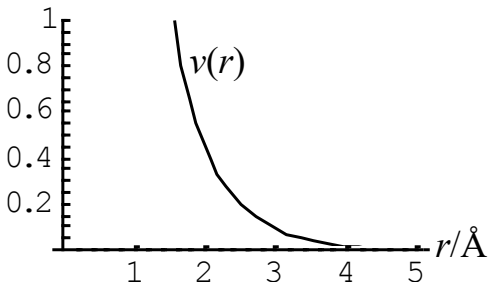

Figure 3: The ghost atom potential $v(r)$ used to obtain the initial and final cage centers as foci of the bipolar coordinate system.

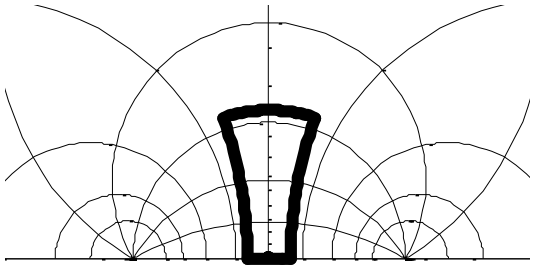

Figure 4: Counting the water molecules within the outlined "volume" in q-θ space determines whether there is a water vacancy between the donor and acceptor cages.

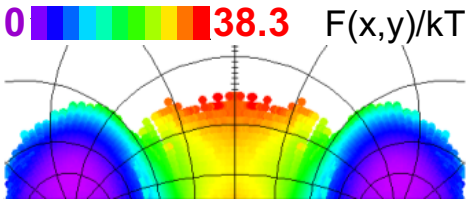

Figure 5: Free energy landscape for L6L hop with no water vacancy. q-isosurfaces are shown decreasing and increasing in intervals of 1/2 from q=0, the plane of symmetry. θ-isosurfaces are shown in intervals of 30° decreasing from θ=180°, the straight line between the donor and acceptor cages. The distance between the cage centers is 5.68 Å.

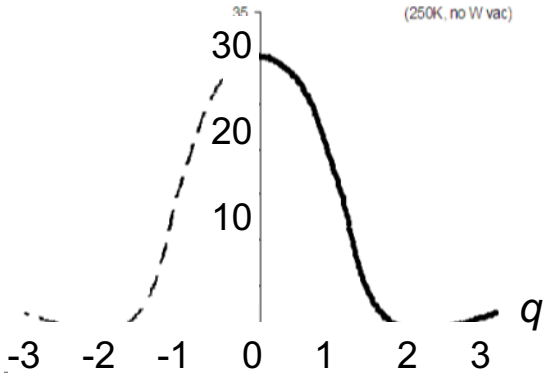

Figure 6: F(q)/kT for the L6L hop with no water vacancy at 250 K. The dotted portion is the symmetric image of the solid $q > 0$ curve.

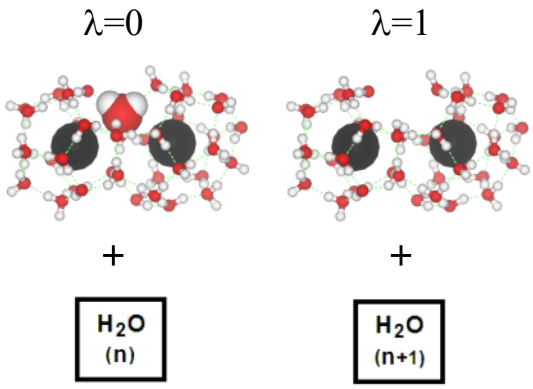

Figure 7: A vacancy in the host lattice of the hydrate was created by thermodynamic integration. The interaction parameters of one TIP4P water molecule were scaled from one to zero in the hydrate lattice and from zero to one in a liquid TIP4P water simulation at 250 K and 40 atm.

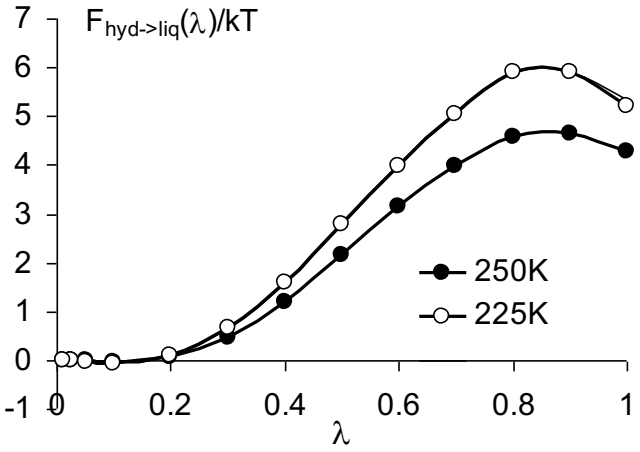

Figure 8: The free energy to create a water vacancy in the hydrate lattice as a function of the coupling parameter λ. The TIP4P molecule was transferred to the equilibrium 40atm phase of TIP4P water (or ice-h) at 250 K and 225 K. The small correction on the last data point at T=225 K is explained in the text.

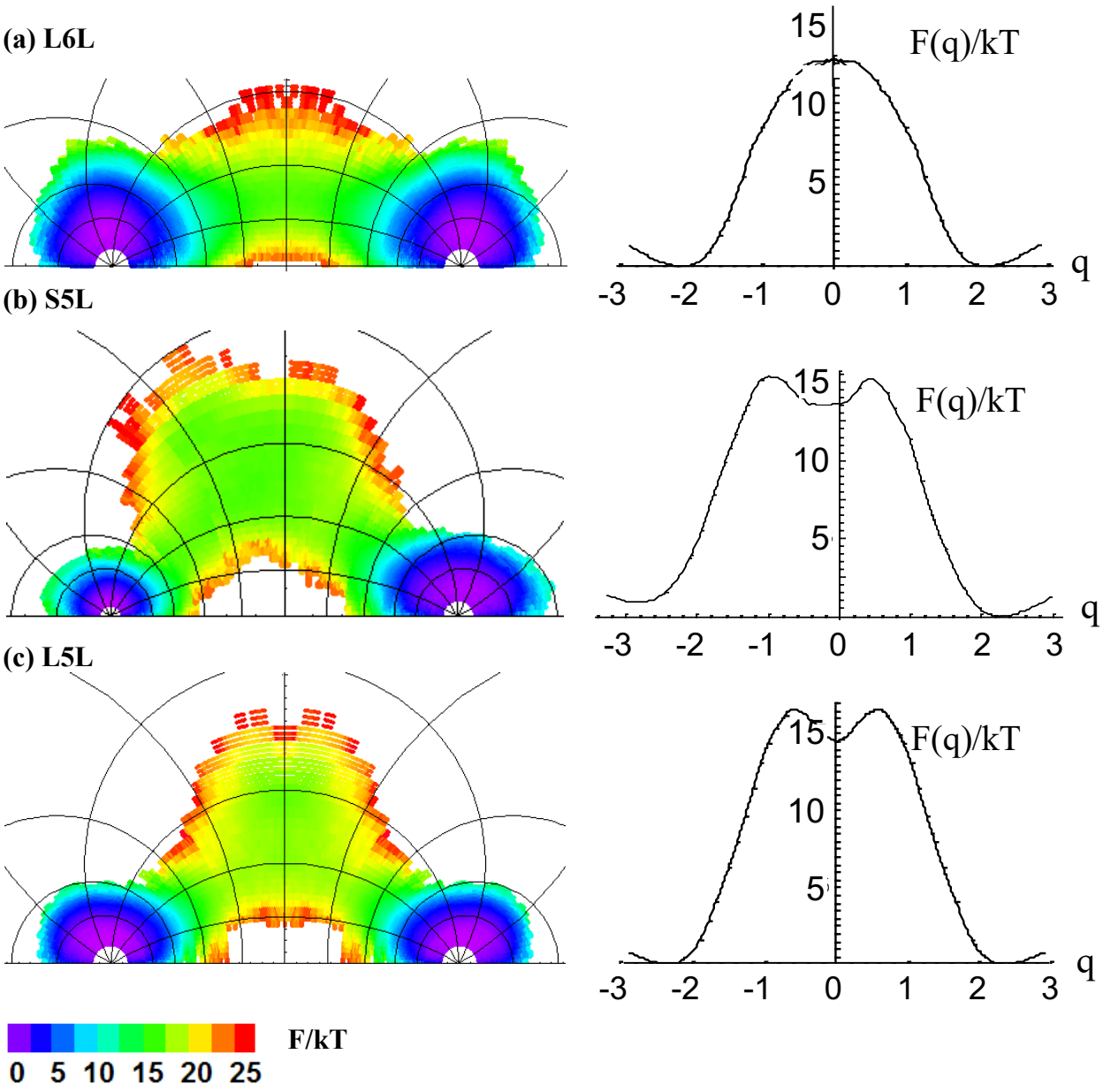

Figure 9: Free energy landscapes at 250K for the L6L(a), S5L(b), and L5L(c) hops. All plots are colored according to the same scale. q-isosurfaces are shown decreasing and increasing in intervals of 1/2 from the q=0 plane of symmetry. θ-isosurfaces are shown in intervals of 30° decreasing from the straight line path between donor and acceptor centers, θ=180°. F(q)/kT is shown to the right of each two-dimensional free energy surface.

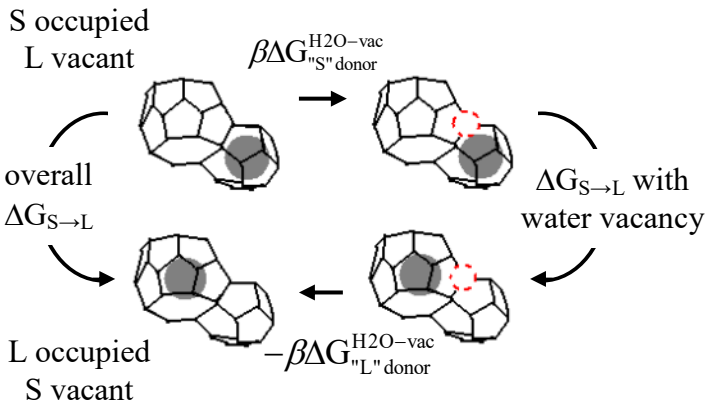

Figure 10: The overall free energy change along the S5L pathway with no water vacancy should correspond to the observed occupation probabilities for the small and large cages. When a water vacancy is introduced, the S5L and L5S pathways require a small correction because the free energy to form and heal the water vacancy before and after methane hopping do not cancel, i.e. because $\beta\Delta G^{H2O-vac}_{"L" donor}$ and $\beta\Delta G^{H2O-vac}_{"S" donor}$ are not equal.

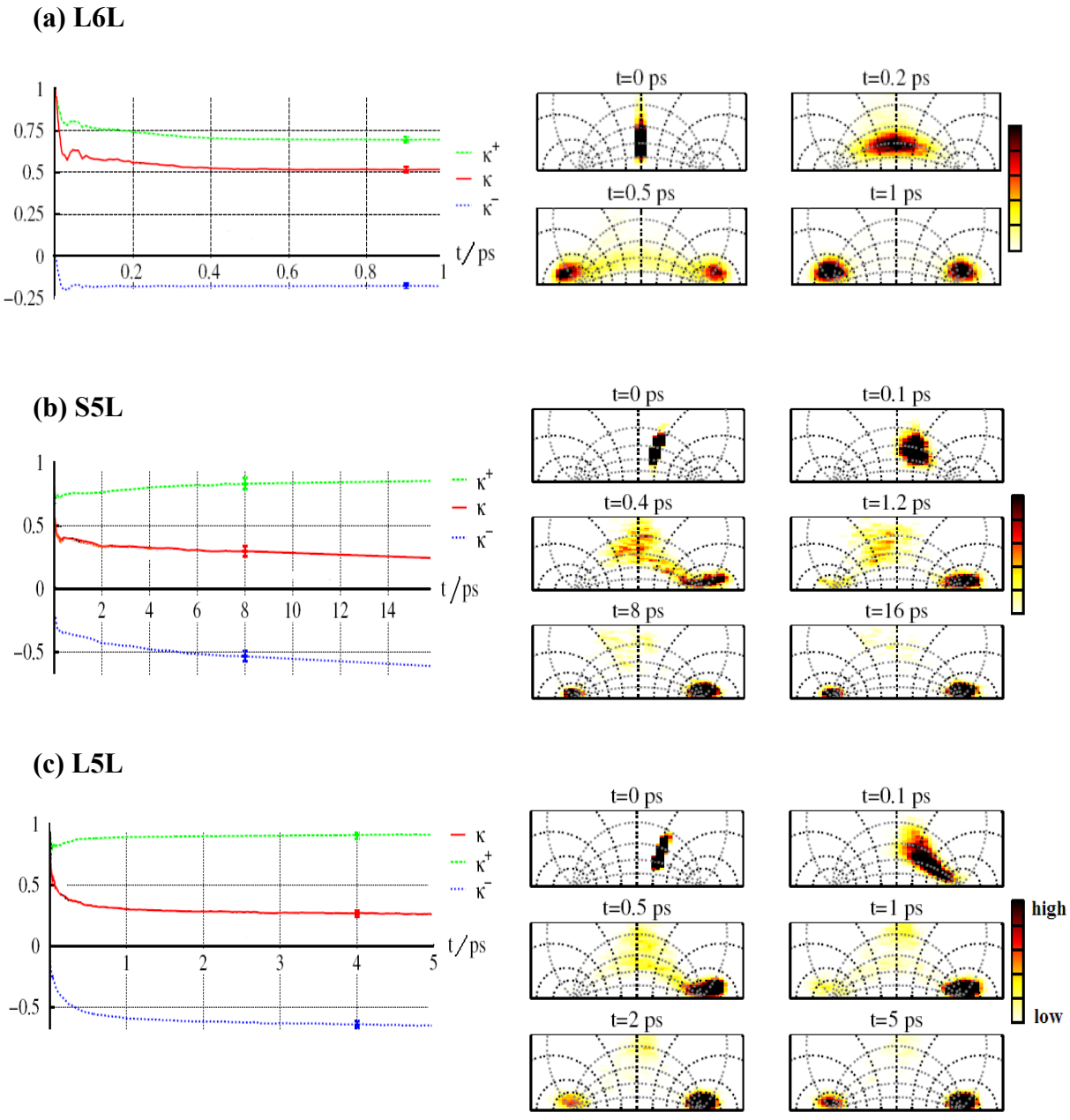

Figure 11(a), (b), and (c): Reactive flux correlation function $\kappa(t)$ for the L6L (a), S5L (b), and L5L (c) hops. Separate contributions to the reactive flux from trajectories that were initially crossing the transition state surface in the forward direction (κ^+) and backward (κ^-) directions are also shown. The evolving density of a swarm of trajectories initiated from the transition state surface is shown next to each correlation function.

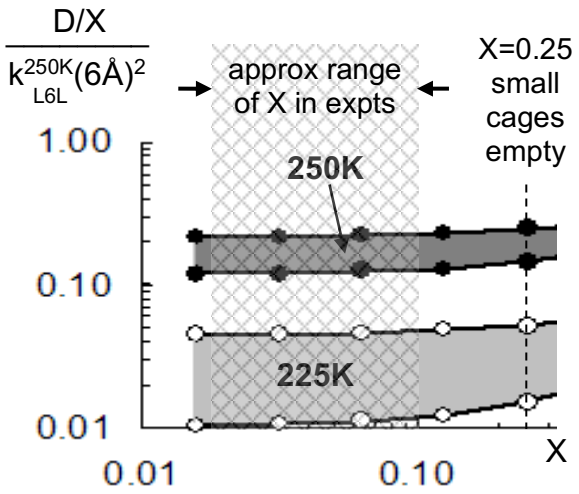

Figure 12: CH_4 self-diffusion rates as a function of X, the fraction of hydrate cages that do not contain a methane molecule. The solid gray regions show the range of values that can result depending on how the correction η is applied. The normalization factor $k_{L6L}(6Å)^2$ is $3.6 \cdot 10^{-14} m^2/s$.

		water vacancy region		
	r_{EQ}/Å	q_{min}	q_{max}	θ_{min}
L6L	5.68	-0.32	0.32	85°
L5L	7.14	-0.32	0.32	95°
S5L	6.59	-0.32	0.16	90°

Table 1: equilibrium distance between ghost atoms, and the values of q and θ that define a region that must contain a water vacancy.

250K	L6L	L5L	L5S	S5L
F_D/kT	0.1	0.2	0.1	0.9
F^*/kT	12.7	16.6	15.3	15.3
$\Delta F/kT$	12.6	16.4	15.2	14.4
q^*	0.00	0.60	0.42	0.42
θ^*	135°	125°	120°	120°
$\beta h\langle\lvert\dot{q}\rvert\rangle_{q^*}$	0.33	0.27	0.27	0.27

225K	L6L	L5L	L5S	S5L
F_D/kT	0.1	0.2	0.4	0.1
F^*/kT	12.8	18.6	16.4	16.4
$\Delta F/kT$	12.7	18.4	16.0	16.3
q^*	0.00	0.60	-0.90	-0.90
θ^*	135°	120°	115°	115°
$\beta h\langle\lvert\dot{q}\rvert\rangle_{q^*}$	0.35	0.27	0.33	0.33

Table 2: Transition state theory parameters at 250K and 225K. The subscript D denotes the free energy of the donor basin: $-\beta F_D = \ln\int dq \exp[-\beta F(q)]$ where integration is over $q < q^*$. q^* is the value of q at the maximum in $F(q)$, and θ^* is the minimum on $q=q^*$ in the free energy landscapes of Figure 9. $\beta h\langle|\dot{q}|\rangle_{q^*}$ is the dimensionless absolute average velocity along q at $q=q^*$.

250K	L6L	S5L	L5L
$n_{trajectories}$	10000	2590	7500
$t_{plateau}$	1ps	16ps	5ps
q^*	0.00	0.45	0.55
$\beta h\langle\lvert\dot{q}\rvert\rangle_{q=q^*}$	0.28	0.49	0.48
$\kappa(t_{plateau})$	0.52	0.29	0.24
$\langle H[q(t_{plateau})]\rangle_{q(0)=q^*}$	0.424	0.722	0.654

Table 3: Summarized transmission coefficient data at 250K. The table also shows numerical estimates of the initial dimensionless absolute velocity along the reaction coordinate and the fraction of trajectories from the initial swarm that commit to the product state.

250K	L6L	L5L	L5S	S5L
ΔF/kT	12.6	16.4	**15.2**-16.1	13.5-**14.4**
κ	0.52	0.24	0.29	0.29
$\beta h\langle\lvert\dot{q}\rvert\rangle_{q^*}$	0.28	0.48	0.49	0.49
k/(ms^{-1})	101.0	1.50	**6.4**-2.6	35.0-**14.2**
225K	L6L	L5L	L5S	S5L
ΔF/kT	12.7	18.4	**16.0**-17.9	14.3-**16.3**
κ	*0.52*	*0.24*	*0.29*	*0.29*
$\beta h\langle\lvert\dot{q}\rvert\rangle_{q^*}$	0.30	0.51	0.52	0.52
k/(ms^{-1})	31.8	0.07	**0.99**-0.14	5.3-**0.74**

Table 4: The activation free energy $\Delta F/kT$, κ, $\beta h\langle|\dot{q}|\rangle_{q^*}$, and rate constants for each pathway. The bold L5S free energy barrier is uncorrected and paired with a corrected (non-bold) S5L free energy barrier. Similarly, the bold S5L barrier is uncorrected and paired with a corrected L5S value. The corrections enforce methane's preference for large cages over small cages as described in the text. The correction is $2kT$ at 225 K and $0.9kT$ at 250 K.

REFERENCES

1 E. D. Sloan, *Clathrate Hydrates of Natural Gases, 2nd Ed.* (Marcel-Dekker, Monticello, NY, 1998).
2 C. A. Koh, Chem. Soc. Rev. **31,** 157 (2002).
3 E. D. Sloan, Nature **426,** 353 (2003).
4 C. A. Koh and E. D. Sloan, AIChE Journal **53,** 1636 (2007).
5 S. Thomas and R. A. Dawe, Energy **28,** 1461 (2003).
6 Y. H. Mori and T. Mori, AIChE Journal **35,** 1227 (1989).
7 M. Ota, Y. Abe, M. Watanabe, R. L. Smith, and H. Inomata, Fluid Phase Equilibria **228,** 553 (2005).
8 P. Dornan, S. Alavi, and T. K. Woo, J. Chem. Phys. **127,** 124510 (2007).
9 S. Takeya, W. Shimada, Y. Kamata, T. Ebinuma, T. Uchida, J. Nagao, and H. Narita, J. Phys. Chem. A **105,** 9756 (2001).
10 T. Uchida, S. Takeya, L. D. Wilson, C. A. Tulk, J. A. Ripmeester, J. Nagao, T. Ebinuma, and H. Narita, Canadian J. of Physics **81,** 351 (2003).
11 W. F. Kuhs, D. K. Staykova, and A. N. Salamatin, J. Phys. Chem. B **110,** 13283 (2006).
12 M. Bach-Verges, S. J. Kitchin, K. D. M. Harris, M. Zugic, and C. A. Koh, J. Phys. Chem. B **105,** 2699 (2001).
13 K. A. Udachin, H. Lu, G. D. Enright, C. I. Ratcliffe, J. A. Ripmeester, N. R. Chapman, and G. Spence, Angew. Chem. Int. Ed. **46,** 8220 (2007).
14 S. A. Klapp, H. Klein, and W. F. Kuhs, Geophysical Research Letters **34,** L13608 (2007).
15 H. Lee, Y. Seo, Y.-T. Seo, I. L. Moudrakovski, and J. A. Ripmeester, Angew. Chem. Int. Ed. **42,** 5048 (2003).
16 R. Radhakrishnan and T. Schlick, J. Chem. Phys. **121,** 2436 (2004).
17 D. Chandler, J. Chem. Phys. **68,** 2959 (1978).
18 D. T. Gillespie, J. Comp. Phys. **28,** 395 (1978).
19 A. Demurov, R. Radhakrishnan, and B. L. Trout, J. Chem. Phys. **116,** 702 (2002).
20 L. F. Shampine, Quart. App. Math. **Oct. ,** 287 (1973).
21 D. W. Davidson and J. A. Ripmeester, in *Inclusion Compounds*; *Vol. 3*, edited by J. L. Atwood, J. E. D. Davies, and D. D. MacNicol (London Academic, Oxford, 1984), p. 69.
22 T. M. Kirschgen, M. D. Zeidler, B. Geil, and F. Fujara, Phys. Chem. Chem. Phys. **5,** 5247-5252 (2003).
23 B. J. Anderson, Fluid Phase Eq. **254,** 144 (2007).
24 B. J. Anderson, J. W. Tester, and B. L. Trout, J. Phys. Chem. B. **108,** 18705 (2004).
25 J. B. Klauda and S. I. Sandler, J. Phys. Chem. B **106,** 5722 (2002).
26 S. Alavi and J. A. Ripmeester, Angew. Chem. Int. Ed. **46,** 6102 (2007).
27 P. M. Rodger, J. Phys. Chem. **94,** 6080-6089 (1990).
28 B. J. Anderson, J. W. Tester, G. P. Borghi, and B. L. Trout, J. Am. Chem. Soc. **127,** 17852 (2005).
29 R. Radhakrishnan and B. L. Trout, J. Chem. Phys. **117,** 1786 (2002).
30 L. A. Baez and P. Clancy, Annals. of NY Acad. Sci. **715,** 177 (1994).

[31] N. J. English and J. M. D. MacElroy, J. Comp. Chem. **24,** 1569 (2003).
[32] G. J. Guo, Y. G. Zhang, and H. Liu, J. Phys. Chem. C **111,** 2595 (2007).
[33] J. S. Tse, M. L. Klein, and I. R. McDonald, J. Chem. Phys. **81,** 6146 (1984).
[34] Y. P. Handa, J. S. Tse, and D. D. Klug, J. Chem. Phys. **94,** 623 (1991).
[35] V. P. Shpakov, J. S. Tse, C. A. Tulk, B. Kvamme, and V. R. Belosludov, Chem. Phys. Lett. **282,** 107 (1998).
[36] W. L. Jorgensen, J. Chandrasekhar, J. D. Madura, R. W. Impey, and M. L. Klein, J. Chem. Phys. **79,** 926 (1983).
[37] E. Sanz, C. Vega, J. L. F. Abascal, and L. G. MacDowell, Phys. Rev. Lett. **92,** 255701 (2004).
[38] C. Vega, E. Sanz, and J. L. F. Abascal, J. Chem. Phys. **122,** 114507 (2005).
[39] T. Darden, D. York, and L. Pederson, J. Chem. Phys. **98,** 10089 (1993).
[40] W. L. Jorgensen, J. D. Madura, and C. J. Swenson, J. Am. Chem. Soc. **106,** 6638 (1984).
[41] V. Buch, P. Sandler, and J. Sadlej, J. Phys. Chem. B **102,** 8641 (1998).
[42] W. G. Hoover, Phys. Rev. A **31,** 1695 (1985).
[43] G. J. Martyna, D. J. Tobias, and M. L. Klein, J. Chem. Phys. **101,** 4177 (1994).
[44] D. Frenkel and B. Smit, *Understanding Molecular Simulation: from Algorithms to Applications, 2nd Ed.* (Academic Press, San Diego, 2002).
[45] B. Peters and B. L. Trout, J. Chem. Phys. **125,** 054108 (2006).
[46] B. Peters, G. T. Beckham, and B. L. Trout, J. Chem. Phys. **127,** 034109 (2007).
[47] P. G. Bolhuis, D. Chandler, C. Dellago, and P. L. Geissler, Ann. Rev. Phys. Chem. **53,** 291 (2002).
[48] G. T. Beckham, B. Peters, C. Starbuck, N. Variankaval, and B. L. Trout, J. Am. Chem. Soc. **129,** 4714 (2007).
[49] G. T. Beckham, B. Peters, and B. L. Trout, J. Phys. Chem. B **112,** 7460 (2008).
[50] G. M. Torrie and J. P. Valleau, J. Comp. Phys. **23,** 187 (1977).
[51] P. K. Weiner and P. A. Kollman, J. Comp. Chem. **2,** 287 (1981).
[52] B. R. Brooks, R. E. Bruccoleri, B. D. Olafson, D. J. States, S. Swaminathan, and M. Karplus, J. Comp. Chem. **4,** 187 (2004).
[53] E. Lindahl, B. Hess, and D. v. d. Spoel, J. Molec. Modeling **7,** 306 (2001).
[54] J. C. Phillips, R. Braun, W. Wang, J. Gumbart, E. Tajkhorshid, E. Villa, C. Chipot, R. D. Skeel, L. Kale, and K. Schulten, J. Comp. Chem. **26,** 1781 (2005).
[55] S. Kumar, D. Bouzida, R. H. Swendsen, P. A. Kollman, and J. M. Rosenberg, J. Comp. Chem. **13,** 1011 (1992).
[56] D. R. Lide, *Handbook of Chemistry and Physics, 88th Ed.* (CRC Press, Boca Raton, FL, 2007).
[57] E. P. van Klaveren, J. P. J. Michels, J. A. Schouten, D. D. Klug, and J. S. Tse, J. Chem. Phys. **114,** 5745 (2001).
[58] P. Hanggi, P. Talkner, and M. Borkovec, Rev. Mod. Phys. **62,** 251 (1990).
[59] G. K. Schenter, B. C. Garrett, and D. G. Truhlar, J. Chem. Phys. **119,** 5828 (2003).
[60] G. A. Korn and T. M. Korn, *Mathematical Handbook for Scientists and Engineers* (McGraw-Hill, New York, 1961).
[61] J. C. Keck, Disc. Faraday Soc. **33,** 173 (1962).
[62] W. H. Miller, J. Chem. Phys. **65,** 2216 (1976).

[63] B. Peters, A. T. Bell, and A. Chakraborty, J. Chem. Phys. **121,** 4453 (2004).
[64] R. A. Kuharski, D. Chandler, J. A. Montgomery, F. Rabii, and S. J. Singer, J. Phys. Chem. **92,** 3261 (1988).
[65] M. T. Kirchner, R. Boese, W. E. Billups, and L. R. Norman, J. Am. Chem. Soc. **126,** 9407 (2004).
[66] T. Uchida, T. Hirano, T. Ebinuma, H. Narita, K. Gohara, S. Mae, and R. Matsumoto, AIChE Journal **45,** 2641 (1999).
[67] Y. Seo, H. Lee, and B. H. Ryu, Geophysical Research Letters **29,** 1244 (2002).
[68] J. A. Ripmeester and C. I. Ratcliffe, J. Phys. Chem. **92,** 337 (1988).
[69] T. J. Gallaway, W. Ruska, P. S. Chappelear, and R. Kobayashi, Ind. Eng. Chem. Fundam. **9,** 237 (1970).
[70] J. L. De Roo, C. J. Peters, R. N. Lichtenthaler, and G. A. M. Diepen, AIChE Journal **29,** 651 (1983).
[71] K. A. Udachin, C. I. Ratcliffe, and J. A. Ripmeester, J. Phys. Chem. B **105,** 4200 (2001).

TABLE OF CONTENTS GRAPHIC